Geochimica et Cosmochimica Acta Vol. 54, pp. 3197–3208

0016-7037/90/$3.00 + .00

Compositions of large metal nodules in mesosiderites: Links to iron meteorite group IIIAB and the origin of mesosiderite subgroups

JAMSHID HASSANZADEH,[1,2] ALAN E. RUBIN,[1] and JOHN T. WASSON[1,2,3]

[1]Institute of Geophysics and Planetary Physics, University of California, Los Angeles, CA 90024, USA
[2]Department of Earth and Space Sciences, University of California, Los Angeles, CA 90024, USA
[3]Department of Chemistry and Biochemistry, University of California, Los Angeles, CA 90024, USA

(*Received April* 10, 1989; *accepted in revised form August* 29, 1990)

Abstract—Large mesosiderite metal nodules were studied petrographically and by neutron activation; their large sizes minimized the effects of silicate contamination and dilution by Fe reduced from FeO. The remarkable mixture of subequal amounts of metal and basaltic and pyroxenitic silicates in mesosiderites can be explained by the accretion of a core-like metal mass from one asteroid onto the surface of another asteroid; our data show that the accreted mass had a composition roughly similar to that of the IIIAB iron-meteorite core, consistent with other evidence of close genetic links between these and other related groups. The siderophile compositional pattern, the very limited compositional range, the (inferred) large projectile/target ratio, and the electrical interconnectedness of mesosiderite metal indicate that the bulk of the metal was molten when accreted. Mesosiderites have been divided into plagioclase- and tridymite-rich subgroup A and orthopyroxene-rich subgroup B on the basis of modal silicate mineralogy. Roughly the same subgroups are defined by metal compositions; Au, As, Ni, and Cu are generally higher, and W lower in subgroup A than in subgroup B. In our sample set, a Widmanstätten pattern is only observed in nodules from subgroup A.

A plausible model is that subgroup A best preserves the compositions of the target regolithic silicates and accreted core; subgroup B is comprised of these materials together with a minor amount of core-mantle materials consisting of olivine and refractory, Ni-poor metal. The independent covariation of Ga, Re, and Ir may in part reflect fractionations during impact heating events. The anomalous mesosiderite Reckling Peak A79015 is strongly depleted in refractory siderophiles and slightly enriched in volatile siderophiles; such evolved metal requires a formation distinct from common mesosiderite metal.

INTRODUCTION

MESOSIDERITES ARE enigmatic meteorites consisting of roughly equal portions of basaltic-pyroxenitic silicates and metal. Models of mesosiderite formation include accretion of the metallic core of one differentiated asteroid onto the basaltic surface of another (POWELL, 1971; WASSON et al., 1974; WOOD, 1979; WASSON and RUBIN, 1985), mixing of basaltic crustal blocks with the molten metallic core of a single body (GREENBERG and CHAPMAN, 1984), and combinations of internal and external processes (DELANEY, 1983).

Chemical and O-isotopic compositional data suggest that the eucrites (Euc), howardites (How), mesosiderites (Mes), main-group pallasites (Pal), and IIIAB irons originated on the same or closely related parent bodies (CHOU et al., 1976; CLAYTON et al., 1976; SCOTT and WASSON, 1976; CLAYTON and MAYEDA, 1978; WASSON, 1985). The relationships among these meteorite groups have been explored by numerous workers.

Mes ^{87}Rb-^{87}Sr studies record ages ranging from 4.2 Ga (RAMA MURTHY et al., 1978) down to 3.6 Ma (MITTLEFEHLDT et al., 1986); ^{39}Ar-^{40}Ar ages are about 3.7 ± 0.1 Ga (BOGARD et al., 1988). Cosmic-ray ages are in the range 30–130 Ma, if the highly uncertain 160 Ma age of Bondoc is neglected (BEGEMANN et al., 1976).

We initiated this study to clarify several points:

1) WASSON et al. (1974) observed positive trends among Ni, Ga, Ge, and Ir concentrations in samples of fine-grained Mes metal. MITTLEFEHLDT et al. (1979) and HARLOW et al. (1982) reported evidence of metamorphic reduction of FeO; variable FeO reduction could generate such positive trends. Because this effect should be most pronounced in the fine Mes metal grains, we attempted to minimize the effect by limiting the present study to large nodules (minimum dimension ≥ 3 mm). If a IIIAB-like composition is preserved, it should be most recognizable in cm-size Mes metal nodules.
2) Some large Mes nodules show Widmanstätten patterns (Fig. 1). It has not been clear previously if these patterns were present in the metal before incorporation of solid core fragments into mesosiderite breccias, or whether they grew *in situ* as a result of annealing in the γ field of the Fe-Ni phase diagram followed by slow cooling through the $\alpha + \gamma$ field. We investigated these possibilities from both a structural and a chemical perspective.
3) WIDOM et al. (1986) found that, relative to fine-grained metal, large metal nodules in H chondrites were severely depleted in refractory siderophiles other than W. An origin by impact-shock-induced distillation was proposed. Because the breccia-within-breccia nature of mesosiderites implies repeated impacts and redox conditions on the H and Mes parent bodies appear to have been roughly similar, we speculated that similar compositional effects might be resolvable in large Mes nodules.
4) WASSON and RUBIN (1985) noted that the Ir/Ni ratio was lower in subgroup-A than in subgroup-B mesosiderites (FLORAN, 1978; HEWINS, 1984). It seemed important to find out whether other elements could be used to resolve the metal in these subgroups.

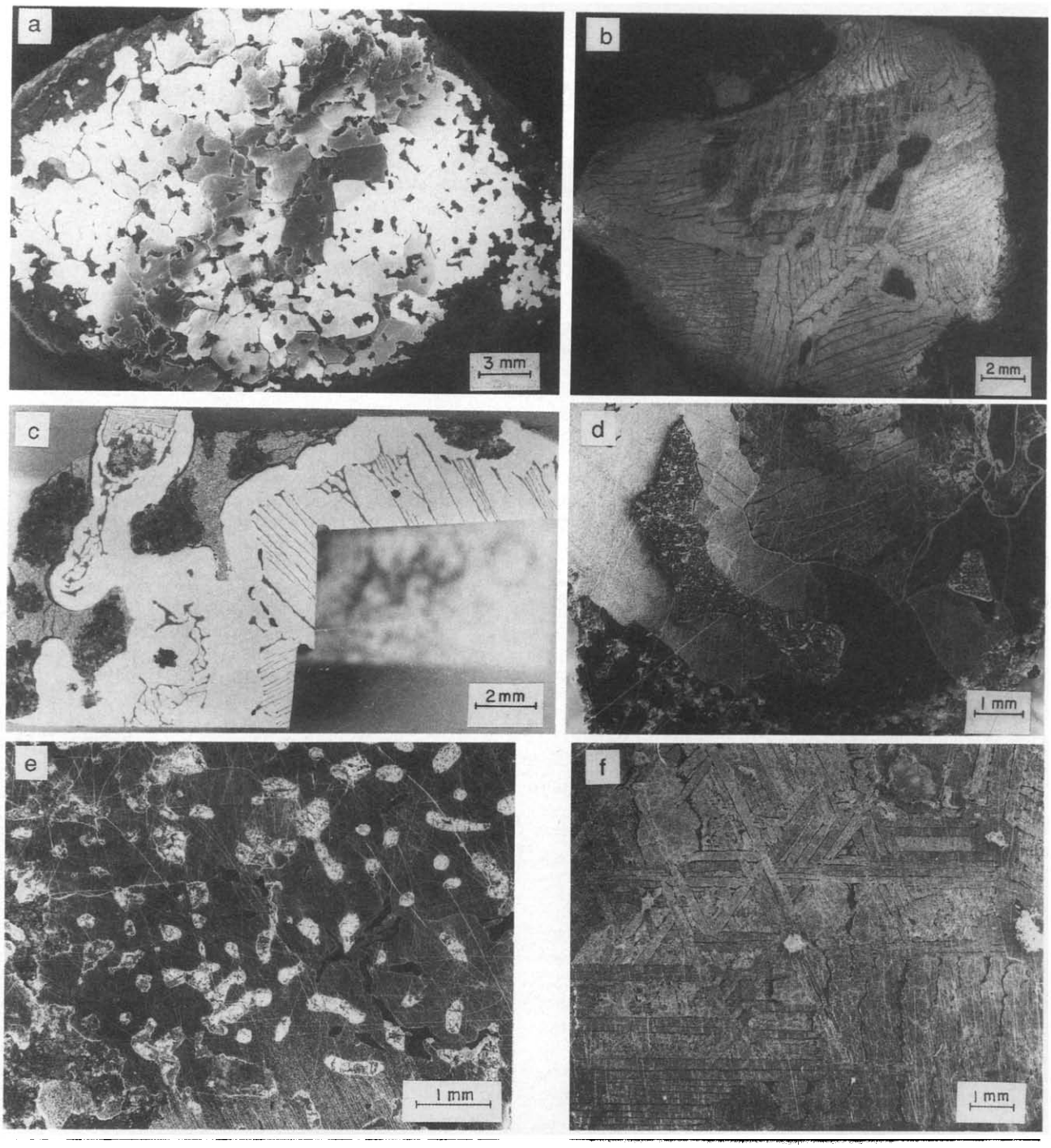

FIG. 1. Macroscopic photographs of mesosiderite nodules (reflected light). (a) The Bondoc nodule is comprised predominantly of polycrystalline kamacite (white to grey); the dark patches between kamacite grains are silicates. (b) The Dalgaranga nodule exhibits a prominent Widmanstätten pattern; the distorted lamellae may have been produced during formation of the associated crater. The two dark patches are silicate. (c) The Pinnaroo nodule shows a broad zone of swathing kamacite around an interior octahedral regin; the area outside the swathing kamacite is composed of troilite (light grey) and silicate (dark grey). (d) The Patwar nodule consists of polycrystalline kamacite (light grey area at left; black area at bottom center) containing troilite (mottled elongated grain at left) surrounding a central core region with a Widmanstätten pattern (top center). (e) Chinquetti is unique among our normal mesosiderite nodules in showing many ellipsoidal troilite inclusions. (f) This 45-g Vaca Muerta nodule shows a well-defined Widmanstätten pattern; troilite and silicates are minor (3 vol% combined).

SAMPLES AND TECHNIQUES

Metal nodules from 12 mesosiderites were analyzed. They range from 3 mm to 4 cm in minimum dimension and from 10 to 200 mg/g in silicate content. Two additional samples, Pennyweight Point (henceforth Pennyweight) and Murchison Downs (henceforth MurchDowns), were originally designated iron meteorites but were recognized as Mes nodules by WASSON et al. (1989). The Reckling

Peak A79015 meteorite (henceforth RKPA79015) is not a typical mesosiderite; it is dominantly metal, silicates accounting for only ~20% of the mass (CLARKE and MASON, 1982).

Pieces of the large nodules were removed by sawing; small nodules were separated from the silicate-rich mesosiderite matrix by a combination of sawing, carving, and drilling. Matrix silicates were removed mechanically to the greatest extent possible. The abundance of the remaining silicates was estimated visually and by calculations using lithophile (Na, Ca, Sc, Mn, Sm) concentrations in the nodules.

Samples and standards were placed into clean vials made of high-density polyethylene and irradiated for 4 h in the nuclear reactor at the University of California, Irvine; the neutron flux was 1.8×10^{12} cm^{-2} s^{-1}. Samples were counted at UCLA on a high-resolution Ge detector with 22% efficiency and 1.75 keV (at 1332 keV) resolution 4 times during the next 4 weeks. We determined Cr, Fe, Co, Ni, Cu, Ga, Ge, As, Sb, W, Re, Ir, Pt, and Au; in those nodules that contained >2% silicates, we also determined Na, Ca, Sc, Mn, and Sm. A detailed discussion of our instrumental neutron activation analysis (INAA) techniques for metallic samples is given in WASSON et al. (1989). All siderophiles are determined to precisions (roughly one relative standard deviation) of ±5–10% except Sb, for which the precisions are 15–30% below ~200 ng/g. Some high Cr contents may reflect contamination by chromite. Replicate analyses were carried out for six mesosiderites; the Estherville replicate is of an independent nodule, the remaining replicates are additional pieces off the first nodules.

With the exception of Emery (for which no additional material was available), samples of adjacent portions of the same nodules were cast in Castolite resin, finely polished, and etched with nital. Metal phases were analyzed with the UCLA automated Cameca "Camebax-microbeam" electron microprobe using crystal spectrometers. Data were corrected following ZAF procedures.

PETROGRAPHY AND MINERALOGY

The metal nodules range in shape from sub-angular to well rounded; detailed petrographic descriptions appear in the Appendix. Nodules characteristically contain millimeter-size crystals of kamacite present as lamellae or equiaxed. Cloudy taenite occurs as irregular patches or as bands parallel to the kamacite. Tetrataenite forms thin rims on the cloudy taenite with one edge abutting kamacite. Several nodules have Widmanstätten structures, the mean thickness (corrected for geometry) of the widest kamacite lamellae being 0.2–0.7 mm; in these cases the octahedral patterns are continuous across the nodule indicating that it was annealed in the γ-iron field long enough to produce a single crystal. All nodules showing continuous octahedral patterns belong to silicate subgroup A (defined below).

A striking contrast is provided by the large, 4-cm Bondoc nodule (Fig. 1a), which consists of randomly oriented granular kamacite with little cloudy taenite. Either the γ-iron fields reached dimensions of only ~3 mm or the nodule was subjected to a treatment (shock?) that led to random growth of kamacite without a taenite template. Veramin, Morristown, Mincy, Emery, and Chinguetti show related structures. All silicate, subgroup-B Mes in our limited set have this structure.

Mean compositions of the kamacite and tetrataenite are listed in Table 1. Kamacite compositions were determined near the centers of lamellae or on large (>0.2 mm) grains except as indicated; Ni concentrations are moderately low (58–65 mg/g), and still lower (50–55 mg/g) near grain margins. These low kamacite Ni contents, like the tetrataenite, are indicators of protracted periods of low-temperature annealing.

Mes tetrataenite Ni and Co concentrations (Table 1) are in the range of 480–530 mg/g and 0.6–0.9 mg/g, respectively.

Table 1. Mean composition of kamacite cores and tetrataenite in metal nodules from 12 mesosiderites; concentrations in mg/g.

	kamacite				tetrataenite			
mesosiderite	pts	Fe	Co	Ni	pts	Fe	Co	Ni
Bondoc	7	926	5.1	65	2	500	0.6	501
Chinguetti	9	928	5.5	65	4	523	1.0	485
Crab Orchard	9	931	5.0	63	5	505	0.6	495
Dalgaranga	10	935	5.3	58*	5	484	0.9	516
Estherville	3	934	5.0	55*	2	489	0.7	510
Mincy	4	940	4.9	54*	2	496	0.7	504
Morristown	3	940	4.8	53	3	495	0.8	505
Patwar	18	935	5.5	61	5	470	0.7	531
Pinnaroo	13	934	5.3	60*	5	521	1.0	483
RKPA79015	3	932	5.3	59	3	505	1.0	499
Vaca Muerta	9	938	5.1	56	6	496	0.8	517
Veramin	8	930	4.9	66	5	507	0.9	494

* values are typical of thin kamacite bands or areas adjacent to cloudy taenite patches.

The uncertainty in these low Co values is ±20% because of the large correction for the Fe K_β interference. Cloudy taenite exhibits compositional gradients; typically, Ni concentrations are ~400 mg/g.

NEUTRON ACTIVATION RESULTS

Our determinations of 11 elements in the 13 Mes nodules are listed in Table 2; duplicate analyses were carried out for six samples. Also listed is a replicate analysis of RKPA79015 carried out in 1985 and mean compositions (from duplicate analyses) of MurchDowns and Pennyweight reported by WASSON et al. (1989).

Our data agree adequately with earlier results of WASSON et al. (1974), BEGEMANN et al. (1976), and BILD et al. (1983). Some elemental concentrations determined in dissolved samples by WASSON et al. (1974) were thought to be low because of inadequate correction for silicate contamination. Corrections for silicate contamination in the present study are more precise because INAA concentrations of lithophile elements offered excellent control. Concentrations of Na, Ca, Sc, Mn, and Sm are listed in Table 3 together with mean concentrations in Mes silicates from MITTLEFEHLDT et al. (1979). The amounts of silicates estimated from these data and listed in the final column are in good agreement with visual estimates of the silicate contents.

In Fig. 2 we compare our present Ni data with those of WASSON et al. (1974) and BEGEMANN et al. (1976). As expected, the relative standard deviation of the new results (10.4% excluding RKPA79015) is considerably smaller than that of the WASSON et al. (1974) set (15%); as discussed below, much of the Ni variation reflects a systematic trend within the Mes. The relative standard deviation of the BEGEMANN et al. (1976) set is 13%, but drops to 3% if the two extreme values are excluded. Excepting Patwar all recent Ni values are higher. The higher mean Ni content of our samples was expected because of their larger dimensions, smaller surface/volume ratios, and smaller degree of silicate contamination. There is evidence for FeO reduction in Mes materials, and the resulting dilution effects should be more pronounced in the finely divided metal. If dilution is the main cause, it would require about 10–15% of the Fe in the fine metal to have been produced by FeO reduction and Fe_3P oxidation.

Table 2. Concentrations of 11 elements in large metal nodules from 15 mesosiderites in two standards, and mean concentrations in normal mesosiderites and in H (high-AuNi) and L (low-AuNi) Mes subgroups.

meteorite	src*	cat. No.	Cr µg/g	Co mg/g	Ni mg/g	Cu µg/g	Ga µg/g	As µg/g	Sb ng/g	W ng/g	Re ng/g	Ir µg/g	Pt µg/g	Au µg/g	sil sbgr	AuNi sbgr
Bondoc	ASU	684	251	4.82	83.4	140	15.5	6.5	70	1160	730	6.34	13.9	1.02	B	L
			930+	4.83	83.8	129	16.9	7.5	110	1420	800	6.25	12.7	0.95		
Chinguetti	MHNP	1586	93	4.76	104.6	235	15.4	8.8	190	970	560	5.10	8.0	1.17	-	H
Crab Orchard	SI	1590	33	4.72	86.4	111	13.5	9.0	140	1090	600	5.29	7.3	1.13	A	L
Dalgaranga	ASU	676.99	12	4.86	102.7	172	12.7	11.9	260	990	600	4.99	8.0	1.37	A	H
			9+	4.85	96.8	176	12.1	10.9	210	970	520	4.88	8.9	1.36		
Emery	SI	5604	1050+	4.95	79.9	109	14.0+	12.2	90	1310	600	4.88	14.7	1.16	A	int
Estherville	UCLA	636	138	4.86	91.7	135	7.8+	9.4	150	990	460	4.01	7.9	1.15	A	int
			1000+	5.10	91.7	127	5.8+	9.6	160	900	460	4.41	10.0	1.17		
Mincy	UCLA	1016	170	4.71	83.5	119	14.0	8.3	100	1220	700	5.44	9.9	0.99	B	L
Morristown	SI	2934	840+	4.82	87.9	130	15.5	10.5	80	1260	680	5.26	13.0	1.14	A	int
MurchDowns°	WAM	12586	221	4.90	91.6	144	13.6	12.5	310	1110	600	4.98	8.9	1.32	-	H
Patwar	UCLA	719	20	5.42	84.2	114	8.5	13.9	250	870	490	3.78	7.2	1.27	A	anom
Pennyweight°	WAM	13626	50	4.69	82.8	104	14.8	8.8	110	1070	690	5.76	8.5	1.07	-	L
Pinnaroo	SI	2312	30	4.93	97.4	157	13.4	12.1	200	1050	640	5.12	9.0	1.20	A	H
			690+	4.85	99.2	321≠	13.8	11.9	210	1080	620	5.23	9.8	1.24		
RKPA79015	MWG	11	83+	4.86	96.3	195	12.3	11.8	240	810	---	0.479+	---	1.37	-	anom
			214+	5.04	90.2	164	12.2+	11.5	260	730	<50	0.280	3.3	1.36		
Vaca Muerta	UCLA	1259	32+	4.87	105.4	199	7.8+	12.2	350	680	540	5.20	7.1	1.41	A	H
			195+	4.83	110.5	208	8.5+	12.3	320	580	630	5.44	7.3	1.43		
Veramin	GITU	--	170	4.86	77.5	110	13.1	7.4	100	1200	580	4.72	8.8	0.90	B	L
mean, normal Mes			260	4.83	90.4	143	13.6	10.0	165	1090	620	5.18	9.7	1.16		
mean, high-AuNi Mes			80	4.85	100.5	183	10.7	11.4	255	950	590	5.10	8.4	1.29		
mean, low-AuNi Mes			180	4.76	82.8	116	14.3	8.7	108	1170	670	5.50	9.6	1.02		
Filomena	SI	1334	204≠	4.54	56.5	145	58.8	4.8	---	2550	240	3.39	21.3	0.608		
NBS 809B	--	--	719	0.2	33.4	1034	9.1	155.	17100	2080	---	---	3.4	0.047		

* Sources of the meteorites are abbreviated as follows: ASU, Arizona State University; GITU, Geophysics Institute, Tehran University; MHNP, Museum d'Histoire Naturelle, Paris; MWG, Meteorite Working Group, NSF; SI, Smithsonian Institution; UCLA, University of California, Los Angeles; WAM, Western Australian Museum.
\+ Assigned 1/2 wt in the mean
≠ Anomalously high value; discarded
° Murchison Downs and Pennyweight Point data are the means listed in Wasson et al. (1989).

We examined the intercorrelations using the multivariate technique of R-mode factor analysis (DIXON, 1981). We excluded RKPA79015 and Patwar from the sample set but included MurchDowns and Pennyweight. We excluded Cr because a few high values torqued the results so profoundly. The factor analysis yielded two dominant factors and one minor one. The elements loading at levels ≥ 0.7 on the first factor are Ni, Cu, Sb, and Au, positively, and W, negatively. Although these trends are qualitatively similar to those produced in the magmatic iron meteorite groups by fractional crystallization, the absence of a negative correlation of Ni and Au with Ir show that such a simple fractionation scheme is not acceptable.

Loading strongly on the second factor are Ga, Re, and Ir. The association of Re with Ir on the second factor extends the close covariation of these two elements within essentially all sets of related meteorite samples; it surely relates to their similar refractory behaviors and their similar strong partitioning into solid Fe-Ni metal. In contrast, the association of volatile siderophile Ga with refractory siderophile Ir is surprising. The strength of the Ga-Ir correlation is strongly enhanced by the very low concentrations observed in Estherville and moderately low concentrations in Vaca Muerta. However, examination of a Ga-Ir diagram shows a well-defined positive trend even if the low Ga contents of Estherville, Vaca Muerta, and the anomalous Patwar nodule are ignored.

Table 3. Concentrations of lithophile elements in mesosiderite metal nodules, and estimated silicate fraction.

meteorite	Na µg/g	Ca mg/g	Sc µg/g	Mn µg/g	Sm µg/g	sil wt.%
Bondoc	217.	9.1	1.20	114.	0.053	8
Chinguetti	4.9	---	---	---	---	<2
Crab Orchard	2.03	<6	<0.055	18.1	0.031	<2
Dalgaranga	<0.149	<7	<0.130	10.8	<0.033	<2
Emery	267.	7.4	3.40	549.	0.080	20
Estherville	22.3	<8	<0.375	53.1	<0.019	<2
Mincy	47.9	5.5	0.460	103.	0.031	4
Morristown	234.	11.5	2.45	233.	0.098	18
Patwar	16.8	<3	0.190	40.0	0.011	<2
Pinnaroo	10.2	<6	<0.500	34.1	0.008	<2
RKPA79015	2.86	<5	0.250	148.	<0.020	<2
Vaca Muerta	0.55	---	---	---	---	<2
Veramin	46.3	15	<0.500	134.	0.015	3
mean Mes sil	1410.	33.6	15.7	3150	0.38	100

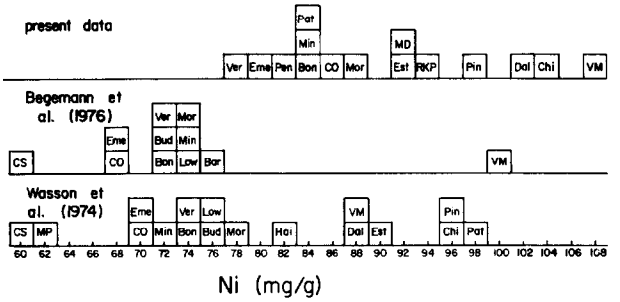

FIG. 2. Histograms of Ni concentrations compare our survey of compositions of large Mes nodules with studies of (mainly) fine Mes metal by BEGEMANN et al. (1976) and by WASSON et al. (1974). Our data on large nodules have higher Ni contents in part because the fine fraction has been diluted by Fe reduced from silicate FeO. However, correction of the earlier data sets for contamination by dissolved silicates could raise the lowest Ni contents to ~80 mg/g.

Although the Ga-Ir correlation can be understood by invoking selective impact volatilization and condensation to produce a metal component of intermediate volatility, such a model currently has too few underpinnings to warrant pursuit.

MESOSIDERITE SUBGROUPS

Following the lead of FLORAN (1978), HEWINS (1984) divided the mesosiderites into A and B subgroups on the basis of the modal silicate mineralogy determined by PRINZ et al. (1980). As summarized by HEWINS (1984), the chief differences between phase volume concentrations in the A and B subgroups, respectively, are orthopyroxene, 55 ± 5 vs. 76 ± 5%; plagioclase, 29 ± 8 vs. 17 ± 4%; and tridymite, 6 ± 2 vs. 2 ± 2%. The A subgroup is dominated by noritic and basaltic clasts which are plagioclase- and tridymite-rich, whereas the B subgroup is dominated by orthopyroxenite. In addition, MITTLEFEHLDT and LINDSTROM (1989) found that incompatible trace elements are ~15% higher in subgroup-A mesosiderites than in subgroup B. Based on the list of HEWINS (1984), our A mesosiderites are Crab Orchard, Emery, Estherville, Morristown, Patwar, Pinnaroo, and Vaca Muerta, and our B samples are Bondoc, Chinguetti,* Mincy, and Veramin. Although HEWINS (1984) did not list Dalgaranga, the PRINZ et al. (1980) modes show it to be type A. The two tiny Australian "irons," MurchDowns and Pennyweight, have not been inserted into this classification scheme because available samples did not preserve adequate amounts of silicates.

WASSON and RUBIN (1985) noted that the WASSON et al. (1974) Mes metal data also resolved the two subgroups; the Ir/Ni ratio is higher in B than in A. The present data on large Mes nodules show differences in mean concentrations between the two silicate subgroups. There are strong positive correlations for Ni, Cu, As, and Au, and negative correlations between these elements and W. Concentrations of Ni, Cu, As, and Au are generally higher in silicate subgroup A than in subgroup B, but the groups are not resolved by these elements. Concentrations of Pt, Re, and Ir show major overlap between A and B. The Ir/Ni differences noted by WASSON and RUBIN (1985) seem mainly to reflect Ni differences between the subgroups.

We applied cluster analysis to a portion of our data set; the set was modified by removing the two samples (Patwar and RKPA79015) having anomalous compositions and the four elements with the greatest scatter—Cr, Ga, Re, and Pt. Because Au is precisely determined and appears to be closely related to the silicate compositional trends, it was given double weight. We employed the algorithm of WILKINSON (1987) using the complete linkage method. This technique emphasizes broad scale relationships as opposed to relationships between individuals. The resulting clusters proved to be quite robust; essentially the same clusters resulted in runs in which Ir alone, W alone, both Ir and W, and Ir, W and, one Au were eliminated from the data matrix.

The resulting dendrogram (Fig. 3) shows that the 13 Mes nodules can be divided into 8 closely related clusters (heavy dotted line) or 3 moderately related clusters (light dotted line). The latter are closely related to the silicate-based A and B subgroups. We designate these three clusters the low-AuNi, high-AuNi, and intermediate-AuNi subgroups; cluster membership is listed in the last column of Table 2. The low-AuNi cluster consists of the tiny Pennyweight iron, three type-B Mes, and one (Crab Orchard) type-A Mes. The high-AuNi cluster consists of the tiny MurchDowns iron, three type A Mes, and Chinguetti (no adequate silicate classification). The three intermediate samples are all type A. Membership in these three subgroups is indicated by different symbols in Fig. 4. Mean compositions of the high-AuNi and low-AuNi subgroups are listed in Table 2.

SIDEROPHILE FRACTIONATION PROCESSES

Siderophiles are essentially unfractionated in chondritic meteorites. For example, data for 22 H-group chondrites obtained by KALLEMEYN et al. (1989) show ranges for Fe, Co, Ni, Ga, As, Os, Ir, and Au that, with few exceptions, are within 10% of the mean values, and much of this scatter can be attributed to sampling errors. In contrast, siderophiles show

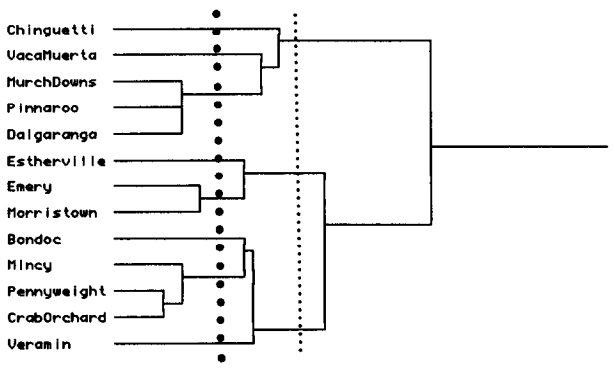

FIG. 3. Dendrogram showing clusters calculated from the concentrations of siderophiles (Co, Ni, Cu, As, Sb, W, Ir, double Au) in our Mes suite (excluding Patwar and RKPA79015); eight clusters are resolved at the position of the heavy dotted line, three at the position of the light dotted line. The latter are designated low-AuNi, high-AuNi, and intermediate subgroups.

* As indicated above, the area (16 mm^2) of the Chinguetti sample of PRINZ et al. (1980) is too small to allow classification; its silicate-based class is, in fact, unknown.

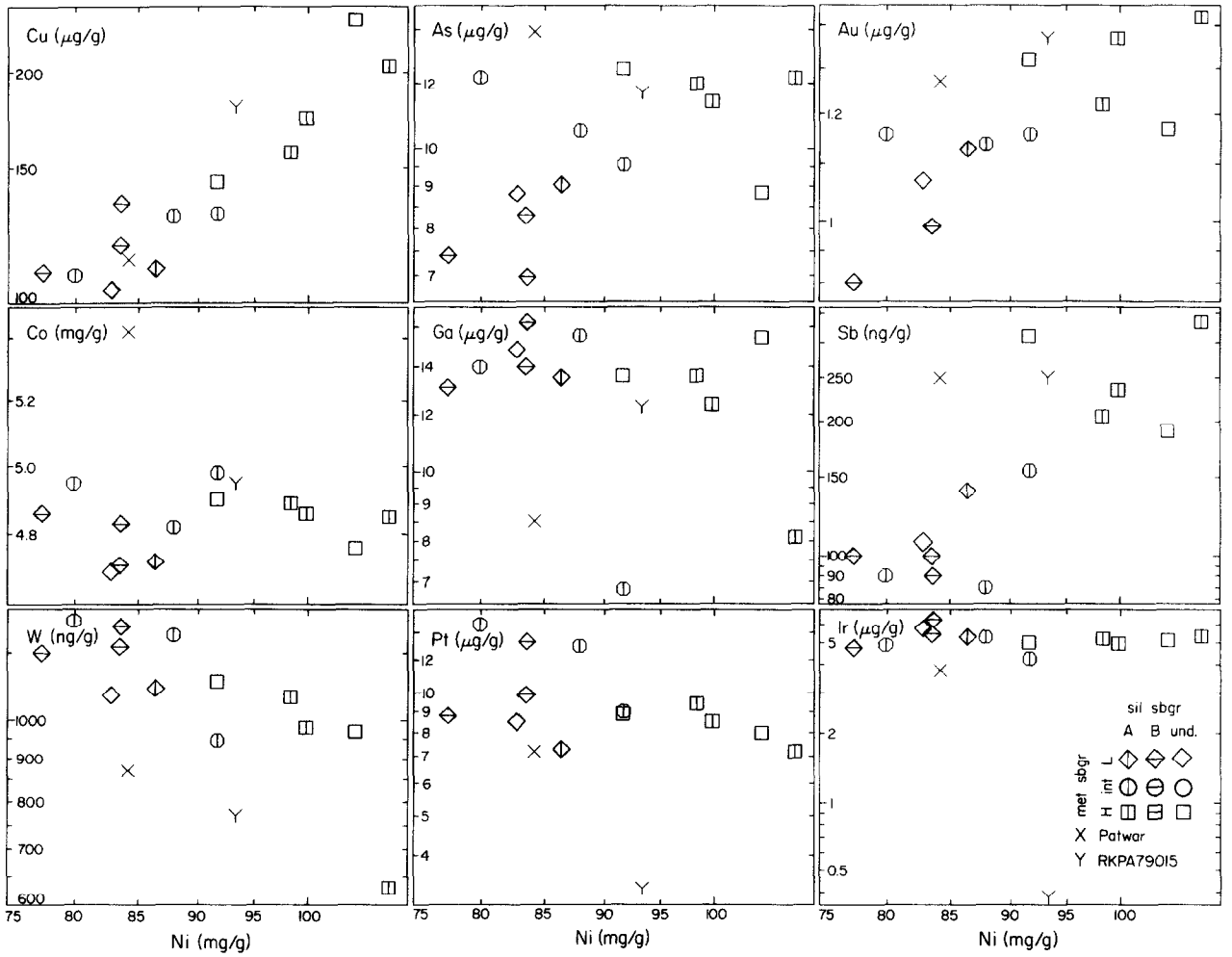

FIG. 4. Element-Ni relationships in large Mes nodules. Open symbols show three subgroups based on metal composition for normal mesosiderites; a vertical line indicates membership in silicate subgroup A, a horizontal line subgroup B. All subgroup B Mes have low metal contents of Ni, Ca, As, Sb, and Au and high contents of W; in most silicate subgroup-A Mes the trend is reversed. The anomalous mesosiderites Patwar and RKPA79015 differ in significant respects from the normal mesosiderites.

large fractionations in those iron-meteorite groups that were formed by fractional crystallization of large magmatic bodies. Groups IIAB and IIIAB are well-sampled examples of such magmatic groups; in each group the maximum/minimum Ir range is ≥2000.

Mean Ni-normalized siderophile abundances in the iron meteorite groups are generally similar to those in chondrites. For example, Fig. VIII-6 of WASSON (1985) shows that (with the exception of poorly constrained Ru) Ni-normalized abundances of strongly siderophile elements are within ±20% of those in H-group chondrites. Abundances of Cu, Ga, Sb, and Ge are 2–3 times lower in IIIAB; this probably reflects loss as volatiles or appreciable partitioning into phases associated with mantle silicates at the time metal segregated to form the parent body core.

If an entire core was accreted onto the surface of the Mes parent body, the bulk composition of the Mes metal should be nominally chondritic. If the core had undergone fractional crystallization and only one portion accreted, interelement siderophile ratios could deviate very widely from chondritic. In group IIIAB, the maximum/minimum Ir/Ni ratios are ~3000, Ir/Au ratios are ~10000, and Ir/As ratios are ~16000. Of course, the range is much smaller if the mean compositions of large core fragments are compared. For example, rough calculations using IIIAB parameters given by WILLIS (1980) show that a fragment representing the g (fraction crystallized) range 0.1–0.2 would have Ir/Au ~ 0.66 times that of the mean core (i.e., mean IIIAB irons), and a fragment representing g = 0.8–0.9 would have Ir/Au ~ 0.005 times the IIIAB mean. These ratios differ by a factor of 130, 100 times less than the range for the entire group, but far larger than the range in chondrites.

In the simplest of possible worlds the compositions of Mes metal nodules would clearly demonstrate that the metal was either (a) uniform and chondritic, (b) uniform and fractionated in a fashion consistent with accretion of a fragment of a differentiated core, or (c) highly variable and consistent with the preservation of the accretion of many small (meter-

size) and diverse fragments from a differentiated core. However, several other minor fractionation processes may have affected the composition of the Mes metal nodules: variable degrees of FeO reduction, diffusional transport on a scale of several centimeters, and volatile transport (and possible loss) on a scale of meters or greater.

The evidence for FeO reduction was recently reviewed by MITTLEFEHLDT (1990); particularly striking was the low FeO contents of mesostasis minerals that would normally have high FeO contents. In some Mes regions tridymite is in close association with kamacite, orthopyroxene (opx), and phosphates (e.g., RUBIN and JERDE, 1987). MITTLEFEHLDT et al. (1979) and NEHRU et al. (1980a) inferred that this resulted from the reduction of FeO out of opx by a reaction such as

$$3\ CaSiO_3 + 5\ FeSiO_3 + 2\ Fe_3P = Ca_3(PO_4)_2 + 8\ SiO_2 + 11\ Fe. \quad (1)$$

The phases are written as endmembers for convenience; Fe would react with preexisting metal to produce kamacite (note that 6/11 of the Fe results from Fe_3P oxidation). Most of this secondary kamacite should now be in the fine metal fraction. Other elements can also be reduced from silicates; after Fe, Co is probably the most likely to show enhanced concentrations in the metal resulting from reduction.

The mesosiderites show evidence of metamorphism for extended periods at high temperatures ($\geq$1400 K) (based on evidence for melting), low temperatures ($\leq$700 K) (based on the growth of tetrataenite), as well as intermediate temperatures (DELANEY et al., 1981). It is plausible that some volatile siderophiles escaped as gases during the high-temperature event that introduced the metal into the basalt or during later thermal events. Among our set of elements, Ga and Sb are probably the most sensitive to loss by volatilization, but Cu, As, and Au are more volatile than the common siderophiles; W is volatile if conditions are sufficiently oxidizing.

SIDEROPHILE COMPOSITIONAL LINKS TO OTHER METEORITE GROUPS

In Fig. 4 we show log-log plots of Mes Co, Cu, Ga, As, Sb, W, Ir, Pt, and Au against Ni. Refractory siderophile contents (e.g., W, Re, Ir, and Pt) are much lower in the RKPA79015 metal than in those of the other nodules. It was on the basis of low Ir and W that MALVIN et al. (1984) designated RKPA79015 to be an anomalous mesosiderite. As shown in Fig. 4, the Co content of the Patwar nodule is about 1.11 times the mean of the other nodules; the maximum/minimum Co range in the other nodules is only 1.05. The Patwar nodule also has the highest As, the second lowest Cr (after Dalgaranga), and the second lowest W, Ir, and Pt (after the anomalous mesosiderite RKPA79015). Because of these anomalous and poorly understood compositional features, we excluded Patwar and RKPA79015 from the set of "normal" nodules that are the basis for most of the following discussion.

Our Emery sample had the highest silicate contamination of any sample and the highest contents of Cr, W, and Pt; thus, the Emery data have larger than average uncertainties. Vaca Muerta has anomalously low contents of Ga and W, and Estherville has low Ga and Ir, but otherwise these Mes nodules fall within the normal fields. The two small meteorites that WASSON et al. (1989) identified as Mes nodules (i.e., Pennyweight and MurchDowns) fall in the normal fields on the compositional diagrams. We include these five meteorites in the normal set.

The Ir range in normal Mes nodules is quite small; the maximum/minimum range is only 6.3/3.8, a factor of 1.7. BILD et al. (1983) reported an Ir range of 6/3 = 2. The small Ir range is grossly inconsistent with the accretion of a large fraction of a fractionally crystallized core, a conclusion also reached by BILD et al. (1983). Because of the great difficulty in rehomogenizing fragments from a large (kilometer-size) body of solid metal by mechanical or diffusional processes (or liquid metal during a brief impact event), it seems highly unlikely that the Ir content of the Mes metal ever spanned a range significantly greater than that now observed.

The best method to estimate the mean composition of a fractionally crystallized iron meteorite group is to fit log-log plots with regression lines, obtain the composition of the first solid from the low-Ni extreme of this line, and infer solid-liquid partition ratios (k_X values) from the slopes ($k_X - 1/k_{Ni} - 1$) and from an estimate of k_{Ni} based on laboratory data. As shown more clearly on an abundance ratio diagram (Fig. 5), the mean IIIAB composition matches that of the normal Mes nodules to within 25% except Re (30% higher than IIIAB), Ga ($\sim$35% lower), and Sb (70% higher). As discussed in more detail below, the high-AuNi cluster may be closer to the primitive endmember of the Mes nodule sequence. The high-AuNi/IIIAB abundance ratios for the well-determined siderophile elements Ir, Co, Au, and As are slightly closer to unity than the Mes/IIIAB mean ratios. H-group abundances (WASSON and KALLEMEYN, 1988) also provide an adequate match to Mes abundances, but the match for IIIAB is closer (Fig. 5).

The similar compositions of metal in Pal and IIIAB irons (SCOTT, 1977), the similar O-isotope compositions in the igneous clan groups Mes, Euc, How, Dio, Pal (CLAYTON et al., 1976), and IIIAB irons (CLAYTON et al., 1986), and the similar FeO/MnO ratios in the silicate fractions of most of these groups imply that the IIIAB irons formed in the core of a parent body closely similar to that which produced the other igneous-clan groups (WASSON, 1985). Following up on the model that calls for formation of Mes by accretion of an iron-meteorite core onto the basaltic surface of an unfragmented asteroid, WASSON and RUBIN (1985) noted that the inferred high projectile/target mass ratio implies a low-accretion velocity (roughly 1 km s^{-1}) and, thus, formation at about the same distance from the Sun early in solar-system history when mean interparticle velocities were low. It seems likely that, at a fixed distance from the Sun, metallic cores in asteroid-size bodies were quite similar in composition; thus, the best a priori candidate for the metallic projectile that accreted to the surface of the Mes body is a IIIAB-like core or core fragment. There are moderate differences in composition between IIIAB and Mes, but these can be explained by plausible ad hoc processes (e.g., loss of Ga as a volatile, gain of Sb by reduction from Fe_3P, etc.). We conclude that Mes and IIIAB are sufficiently related compositionally to have originated in the same narrow region of the solar system.

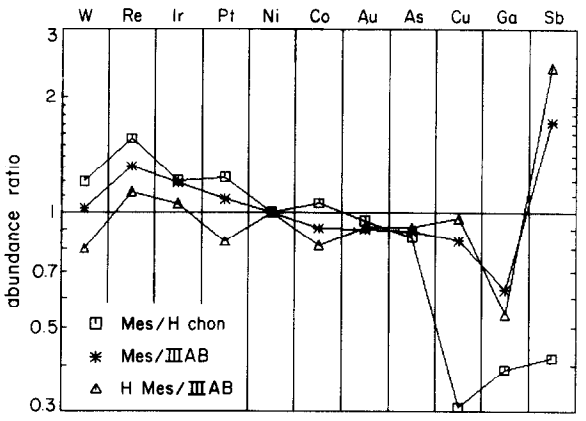

FIG. 5. Ni-normalized siderophile abundances in mesosiderites are similar to those in H chondrites and in the IIIAB core. Elements are ordered in terms of volatility increasing to the right; appreciable deviations are observed only for the three most volatile and/or chalcophile elements Cu, Ga, and Sb. Abundances of the well-determined strongly siderophile elements Ir, Ni, Cu, As, and Au in high-AuNi subgroup mesosiderites (H Mes) closely resemble those in IIIAB.

EVIDENCE FOR ACCRETION OF A MOLTEN CORE

Recalling that Au and Ir experience opposite fractionations during crystallization, we note that the small max/min range in Ir/Au ratios (a factor of ~1.9; 1.8 excluding Patwar) among the Mes nodules further supports the conclusion that the metal that accreted to different parts of the Mes body did not differ appreciably in composition. This has important implications; even adjacent IIIAB-like core fragments representing crystallized fractions $0.1 < g < 0.2$ and $0.2 < g < 0.3$ (each fragment subsequently homogenized) would have max/min Ir/Au ratios ~ 3.

As discussed by WASSON and RUBIN (1985) and references cited therein, the simplest and, in our opinion, most plausible class of model to account for the very high metal fraction of mesosiderites involves accretion of a core. Accretion of an undifferentiated chondritic body is not possible because the mean metal fraction of chondrite groups does not exceed 250 mg/g, and the anticipated large chondritic silicate component is not present. WASSON et al. (1980) proposed that IAB and IIICD irons formed in chondritic megaregoliths as shock melts and solidified too rapidly to undergo fractional crystallization. It seems doubtful that such metallic materials are a reasonable source of Mes metal because the chondritic silicates should also be present in the same cm- to m-scale regions.

These considerations lead us to consider the accretion of a metallic core during the period when it was still molten. Four arguments support such a model:

1) All parts of a molten, homogeneous core would have "chondritic" siderophile abundances, as observed in the mesosiderites.
2) As noted by WASSON and RUBIN (1985), the low accretional velocity postulated to allow the observed high projectile/target ratio is most easily obtained when the inner protoplanets are still small very early in solar system history (perhaps during the first 100 Ma), and it is precisely during these early periods that most cores are expected to be molten.
3) The electrical interconnectedness of mesosiderite metal (POWELL, 1971) is most easily explained by the accretion of a metallic magma.
4) The generally small (millimeter) size of Mes metal grains is unlikely to be produced by regolithic grinding (because of the metal's ductility), but seems understandable in terms of impact spattering of a molten core.

The compositional data on "normal" Mes metal nodules, thus, seem best understood in terms of the accretion of a molten core having a composition closely similar to that of the (entire) iron meteorite group IIIAB. The conclusion implies that the uniform Widmanstätten pattern in several large Mes metal nodules formed by long-term *in situ* annealing in the γ-iron field. In some cases (e.g., Pinnaroo, Fig. 1c), the observed structures show broad swathing kamacite on the exterior implying *in situ* crystallization rather than formation by fragmentation of large "meteoritic" masses. The long term annealing seems best accounted for by deep burial under a hot insulating megaregolith.

COMPONENTS MIXED DURING MESOSIDERITE FORMATION

The general covariation of silicate and metal compositional characteristics suggests that these features were established in the same process or in linked processes. The most obvious model is mixing of materials similar to the observed endmembers: one with plag-rich silicates and Au-poor, W-rich metal, the other with opx-rich silicates and Au-rich, W-poor metal. Closer examination, however, shows the simplicity of this model to be more apparent than real. In order to make this mixing process produce mesosiderites having equal weight fractions of silicates and metal, we need endmembers which also contain similar weight fractions of these two components. In effect, the model consists of mixing two different kinds of mesosiderites, an unsatisfying solution considering the a priori improbability of mixing crustal basalts and "core" metal.

Alternatively, we attempted to account for the trends by FeO reduction following the suggestions of MITTLEFEHLDT et al. (1979) and NEHRU et al. (1980a,b). Such a picture suggests that high-AuNi metal approximates the primitive composition of the metal, and low-AuNi metal is produced from such metal by adding a mass of Fe (from FeO, Fe_3P, FeS) equivalent to 0.4–0.5 times that of the original mass. This leads to concentrations of the diluted elements in subgroup-B metal ~ 0.7 times those in high-AuNi metal. The high W and Cr contents of subgroup-B metal could be attributed to the high-temperature reduction of oxidized forms of these elements and subsequent incorporation into the metal. However, this model fails to predict the silicate compositions. A greater degree of reduction of subgroup-B mesosiderites requires greater amounts of free silica and lower amounts of pyroxene (Eqn. 1), exactly the opposite of the observed trend.

Our third and seemingly most plausible model involves making subgroup-B materials from the mix that produced subgroup-A materials but with the addition of significant amounts of lower-mantle- or core-mantle-interface materials from the projectile parent body. This model bears some resemblance to that of PRIOR (1918), who suggested that me-

sosiderites formed when a pallasitic magma invaded a eucritic magma. As discussed by WASSON and RUBIN (1985), the accretion of metallic core material must have been accompanied by the accretion of mantle materials consisting to a large degree of olivine. At all mesosiderite locations the mass of accreted metal was clearly much larger than that of olivine; however, variations in the olivine/metal ratio could account for the observed differences provided that (1) the subgroup-B materials accreted a larger fraction (25 ± 5% more) of olivine,† and (2) that the olivine was accompanied by refractory metal having moderately low contents of Au, As, and Ni. This is precisely the composition of metal that would remain as a residue from partial fusion. The first metal crystallizing from a core would have a similar but less extreme composition, and would also be a possible diluent. Because the Ir contents of Mes and IIIAB metal are similar (Fig. 5), the amount of core crystallization that could have occurred is ≤5%, leading to an Ir concentration in the residual melt ≥ 0.85 times that in the original core. The difficulty with solid core material is that it would be massive and not intimately associated with the mantle olivine and (1) would, thus, be more difficult to homogenize with the main (molten) metal source, and (2) would not necessarily lead to the strong correlation of A metal with A silicates, etc. For this reason, we think it more probable that the material was a cm-scale mixture of olivine and metal having high W and Ir (in contrast to the low Ir concentrations of main-group pallasites) and low Ni and Au.

According to this picture, the extra olivine at the B site reacts with the reducing agent (assumed to be Fe_3P) and/or with tridymite to form orthopyroxene. At the A site, the fraction of mantle olivine in the original mixture is much lower, and an appreciable amount of the orthopyroxene in the basaltic target is reduced to tridymite plus metallic Fe. Dilution of the metal by freshly reduced Fe is not appreciably different at the A and B sites. The accreted olivine probably had a relatively low FeO/(FeO + MgO) ratio near 0.1, similar to typical values found in pallasites and in some large olivine clasts in mesosiderites (see WASSON and RUBIN, 1985). This is consistent with the observation of HEWINS (1984) that the mean Fs content of subgroup-B orthopyroxene is slightly lower than that in subgroup A. The absence of a negative correlation between Ir and Au suggests that Ir concentrations are dominated by small-scale heterogeneities rather than the large-scale differences responsible for the correlations of Ni and Au with other elements.

THE ANOMALOUS MESOSIDERITE RKPA79015

Reckling Peak A79015 is classified as a mesosiderite because its silicates include the principal Mes phases and phase compositions, the O-isotope composition of its silicate ($\delta^{17}O$ = 1.16, $\delta^{18}O$ = 2.89‰; R. N. CLAYTON, priv. comm.) is in the Mes range, and concentrations of nonrefractory siderophiles in the metal are within or near the Mes range (Fig. 4). It is designated an anomalous mesosiderite because its metal content is above the Mes range (CLARKE and MASON, 1982), and its metal has much (3–10 times) lower contents of Ir and other refractory siderophiles (MALVIN et al., 1984; Fig. 4).

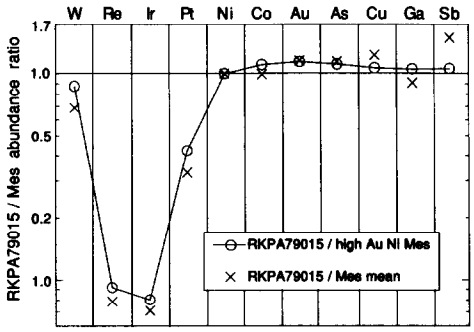

FIG. 6. Ni-normalized siderophile abundances in RKPA79015 differ from mean abundances in normal mesosiderites and also from those in the high-AuNi subgroup. Refractory abundances, particularly Re and Ir are much lower, whereas Co and volatile siderophile abundances are somewhat higher. The RKPA79015 pattern is more compatible with fractional crystallization than with the distillation-condensation proposed by WIDOM et al. (1986) to account for the mechanism patterns in large H-group metal nodules.

WIDOM et al. (1986) discovered that large metal nodules in H chondrites have exceptional abundance patterns in which Ir and Re are depleted by ~100 times relative to bulk fine-grained metal, whereas abundances of other strongly siderophile elements including refractory *W* are 0.8–1.0 times those in the whole rock. These metal nodules were inferred to have formed by local impact-induced heating and fractionation. The depletion of refractories was attributed to partial distillation of chondritic metal producing the nodules as condensates; Ir remained in the residue, the volatility of *W* was enhanced because the environment was moderately oxidizing.

We speculated that the Ir depletion in RKPA79015 might have resulted from a similar process; Mes and H-group metal are similar in composition, but FeO/(FeO + MgO) ratios in Mes silicates are moderately higher indicating that conditions were slightly more oxidizing in the Mes than in the H regolith. In Fig. 6 we plot the ratio of RKPA79015 Ni-normalized abundances to those in normal Mes metal. The RKPA79015 pattern differs in important details from those in the WIDOM et al. (1986) H-group nodules; *W* is 20% lower and the volatile siderophiles are 35–50% higher (and above unity). Normalization to high-AuNi Mes (Fig. 6) reduces these differences but does not eliminate them; however, it also reduces the Ir depletion, the factor rising from 0.055 to 0.070. Thus, the relationship of RKPA79015 to the H-group nodules is weak, and this model does not warrant further discussion.

Because *W* was so high, and the Au and As abundance ratios were <1, the patterns observed by WIDOM et al. (1986) were impossible to explain by a fractional crystallization model. In contrast, the RKPA79015 pattern can be understood in this way, particularly if one allows for our poor knowledge regarding the correct normalization standard. However, ≥95% of the metal would need to crystallize to form the RKPA79015 source, and there is no basis for sug-

† POWELL (1971) analyzed the silicate portions of subgroup-A and -B silicates by X-ray fluorescence. We used these data to determine that addition of ~25 wt% of Fa 11 olivine to mean subgroup-A silicates yields a bulk major element composition that it is similar to (within 5–25% relative of) the mean subgroup-B composition on an FeO-free basis.

gesting that it formed in the same regolith as the normal mesosiderites.

SUMMARY

Our discovery that mesosiderite subgroups based on metal compositions are virtually the same as those based on silicate compositions has important implications regarding the nature of the main materials that were mixed in the mesosiderite regolith. Perhaps the most important of these is that some parts of the projectile may have included a minor core-mantle-boundary component that consisted of refractory metal and forsteritic olivine that, after assimilation, increased the modal fraction of orthopyroxene in the silicates. Most of this olivine seems to have reacted with the basaltic silicates of the target, but a few Mg-rich olivine nodules (e.g., with Fa ~10) may be surviving relicts from this major accretionary event.

Our other main observation is that the narrow range of Mes metal compositions, particularly the Au/Ir ratio, implies that the core of the accreted projectile was largely (≥95%) molten at the time of impact. A molten core helps explain other features of mesosiderites—the uniform dispersal of >90% of metal as small (<2 mm) grains, the electrical interconnectedness of the metal, and the high regolith temperatures that led to the melting of substantial portions of many mesosiderites. More Mes nodules need to be studied in order to better assess the source of the nonsystematic variations in some siderophiles such as Co, Pt, and even Ir.

Our research group's picture of the formation of mesosiderites has evolved in significant ways from that stated by WASSON and RUBIN (1985). We find evidence that the metal was molten at the time of accretion, and, as a result, we hold it to be more likely that an entire small asteroid was accreted to the large asteroid that produced the dominant basaltic component. Our evidence for a correlation between metal and silicate compositions implies that in some regions a minor fraction of the accreted matter consisted of forsteritic olivine and metal having high refractory contents and low Ni, Cu, As, and Au contents; Mes formed in these regions were enhanced in low-AuNi metal and in high-orthopyroxene, low-tridymite silicates.

We suggest the following mesosiderite formation model:

1) At a location in the inner solar system an undefined heat source led to the differentiation of asteroids into metallic cores, peridotitic mantles, and basaltic crusts very early in solar system history (i.e., during the first 100 Ma).
2) An asteroid with a molten core accreted at low velocity (ca. 1 km s^{-1}) onto the basaltic surface of a neighboring asteroid; because these asteroids formed at the same time and same distance from the Sun their bulk compositions were similar.
3) Some of the resulting regions of the "mesosiderite" parent body had high olivine contents, some had high metal contents, others preserved the record of crustal or near-crustal materials; stochastic processes combined with variable resistance to space erosion has resulted in the Earth accreting an unrepresentatively high fraction of mesosiderite materials.
4) The mesosiderite layer was covered with a dry, hot, insulating megaregolith and cooled very slowly.
5) After (and possibly during) cooling slowly enough to produce the highly annealed, tetrataenite-rich metal, a series of impact events produced the observed multiple generations of breccias.
6) One late, massive impact event 3.7 Ga ago produced enough heating to reset the ^{39}Ar-^{40}Ar clocks (BOGARD et al., 1988).
7) More than 130 Ma ago, a km-size mesosiderite fragment entered (or remained in) an orbit that was Earth-crossing or could become Earth-crossing within several Ma; impact erosion of this body produces the observed flux of mesosiderite meteoroids.

Acknowledgments—We thank R. E. Jones, J. Ma, X. Ouyang, and T. Jen for technical assistance; R. N. Clayton for his unpublished O-isotope analysis of RKPA79015; and R. S. Clarke, C. B. Moore, H. Pedersen, P. Pellas, A. W. R. Bevan, and T. B. Thomas for provision of the samples. R. W. Bild, D. W. Mittlefehldt, R. S. Clarke, R. H. Hewins, and E. R. D. Scott generously shared ideas and observations with us. We thank C. R. Chapman and M. Prinz for useful and spirited reviews. This work was supported in part by NASA grant NAG 9-40.

Editorial handling: R. A. Schmitt

REFERENCES

BEGEMANN F., WEBER H. W., VILCSEK E., and HINTENBERGER H. (1976) Rare gases and ^{36}Cl in stony-iron meteorites: Cosmogenic elemental production rates, exposure ages, diffusion losses, and thermal histories. *Geochim. Cosmochim. Acta* **40,** 353–368.

BILD R. W., ROBINSON K. L., SCOTT E. R. D., and PRINZ M. (1983) Origins of mesosiderites as inferred from instrumental neutron activation analysis of their metallic Fe, Ni (abstr.). *Meteoritics* **18,** 266–267.

BOGARD D., MITTLEFEHLDT D., and JORDAN J. (1988) ^{39}Ar-^{40}Ar dating of mesosiderites: A case for major parent body disruption less than 4.0 Gy ago? (abstr.). *Lunar Planet. Sci.* **19,** 112–113.

CHOU C.-L., BOYNTON G. W., BILD R. W., KIMBERLIN J., and WASSON J. T. (1976) Trace element evidence regarding a chondritic component in howardite meteorites. *Proc. Lunar Sci. Conf. 7th,* 727–742.

CLARKE R. S. and MASON B. (1982) A new metal-rich mesosiderite from Antarctica, RKPA79015. *Mem. Natl. Inst. Polar Res., Spec. Issue* **25,** 78–85.

CLAYTON R. N. and MAYEDA T. K. (1978) Genetic relations between iron and stony meteorites. *Earth Planet. Sci. Lett.* **40,** 168–174.

CLAYTON R. N., ONUMA N., and MAYEDA T. K. (1976) A classification of meteorites based on oxygen isotopes. *Earth Planet Sci. Lett.* **30,** 10–18.

CLAYTON R. N., MAYEDA T. K., PRINZ M., NEHRU C. E., and DELANEY J. S. (1986) Oxygen isotope confirmation of a genetic association between achondrites and IIIAB iron meteorites. *Lunar Planet Sci.* **17,** 141–142.

DELANEY J. S. (1983) The formation of mesosiderites, pallasites and other metal-silicate assemblages: two mechanisms (abstr.). *Meteoritics* **18,** 289–290.

DELANEY J. S., NEHRU C. E., PRINZ M., and HARLOW G. E. (1981) Metamorphism in mesosiderites. *Proc. Lunar. Planet. Sci. Conf.* **12B,** 1315–1342.

DIXON W. J. (1981) *BMDP Statistical Software.* Univ. Calif. Press, Berkeley.

FLORAN R. J. (1978) Silicate petrography, classification, and origin of the mesosiderites: Review and new observations. *Proc. Lunar Planet. Sci. 9th,* 1053–1081.

GREENBERG R. and CHAPMAN C. R. (1984) Asteroids and meteorites: origin of stony-iron meteorites at mantle-core boundaries. *Icarus* **57,** 267–279.

HARLOW G. E., DELANEY J. S., NEHRU C. E., and PRINZ M. (1982) Metamorphic reactions in mesosiderites: Origin of abundant phosphate and silica. *Geochim. Cosmochim. Acta* **46,** 339–349.

HEWINS R. H. (1984) The case for a melt matrix in plagioclase-POIK mesosiderites. *Proc. Lunar Planet. Sci. Conf. 15th*, C289–C297.
KALLEMEYN G. W., RUBIN A. E., WANG D., and WASSON J. T. (1989) Ordinary chondrites: Bulk compositions, classification, lithophile-element fractionations and composition-petrographic type relationships. *Geochim. Cosmochim. Acta.* **53**, 2747–2767.
MALVIN D. J., WANG D., and WASSON J. T. (1984) Chemical classification of iron meteorites—X. Multielement studies of 43 irons, resolution of group IIIE from IIIAB, and evaluation of Cu as a taxonomic parameter. *Geochim. Cosmochim. Acta* **48**, 785–804.
MCSWEEN H. Y. (1987) *Meteorites and their Parent Planets.* Cambridge University Press.
MITTLEFEHLDT D. W. (1990) Petrogenesis of mesosiderites: I. Origin of mafic lithologies and comparison with basaltic achondrites. *Geochim. Cosmochim. Acta* **54**, 1165–1173.
MITTLEFEHLDT D. W. and LINDSTROM M. M. (1989) Geochemistry and petrogenesis of mesosiderite whole rock silicates (abstr.). *Lunar Planet. Sci.* **20**, 699–700.
MITTLEFEHLDT D. W., CHOU C.-L., and WASSON J. T. (1979) Mesosiderites and howardites: Igneous formation and possible genetic relationships. *Geochim. Cosmochim. Acta* **43**, 673–688.
MITTLEFEHLDT D. W., BANSAL B. M., SHIH C.-Y., WIESMANN H., and NYQUIST L. E. (1986) Petrology, chronology and chemistry of basaltic clasts from mesosiderites (abstr.). *Lunar Planet. Sci.* **17**, 553–554.
NEHRU C. E., PRINZ M., DELANEY J. S., HARLOW G. E., and FRISHMAN S. (1980a) Gabbroic and basaltic clasts in mesosiderites: unique achondritic tridymite-physphate-rich, two-pyroxene rock types (abstr.). *Lunar Planet. Sci.* **11**, 803–805.
NEHRU C. E., DELANEY J. S., HARLOW G. E., and PRINZ M. (1980b) Mesosiderite basalts and the eucrites (abstr.). *Meteoritics* **15**, 337–338.
POWELL B. N. (1971) Petrology and chemistry of mesosiderite—II. Silicate textures and compositions and metal-silicate relationships. *Geochim. Cosmochim. Acta* **35**, 5–34.
PRINZ M., NEHRU C. E., DELANEY J. S., HARLOW G. E., and BEDELL R. L. (1980) Modal studies of mesosiderites and related achondrites including the new mesosiderite ALHA77219. *Proc. Lunar Planet. Sci. Conf. 11th*, 1055–1071.
PRIOR G. T. (1918) On the mesosiderite-grahamite group of meteorites: with analyses of Vaca Muerta, Hainholz, Simondium, and Powder Mill Creek. *Mineral. Mag.* **18**, 151–172.
RAMA MURTHY V., ALEXANDER E. C., JR., and SAITO K. (1978) Rb-Sr and ^{40}Ar-^{39}Ar systematics of the Estherville mesosiderite (abstr.). *Lunar Planet. Sci.* **9**, 781–783.
RUBIN A. E. and JERDE E. A. (1987) Diverse eucritic pebbles in the Vaca Muerta mesosiderite. *Earth Planet. Sci. Lett.* **84**, 1–14.
SCOTT E. R. D. (1977) Geochemical relationships between some pallasites and iron meteorites. *Mineral Mag.* **41**, 265–272.
SCOTT E. R. D. and WASSON J. T. (1976) Chemical classification of iron meteorites—VII. Groups IC, IIE, IIIF and 97 other irons. *Geochim. Cosmochim. Acta* **40**, 103–115 (1976).
WASSON J. T. (1985) *Meteorites: Their Record of Early Solar-System History.* Freeman.
WASSON J. T. and KALLEMEYN G. W. (1988) Compositions of chondrites. *Phil. Trans. Roy. Soc. London* **325A**, 535–544.
WASSON J. T. and RUBIN A. E. (1985) Formation of mesosiderites by low-velocity impacts as a natural consequence of planet formation. *Nature* **318**, 168–170.
WASSON J. T., SCHAUDY R., BILD R. W., and CHOU C. L. (1974) Mesosiderites—I. Compositions of their metallic portions and possible relationship to other metal-rich meteorite groups. *Geochim. Cosmochim. Acta* **38**, 135–149.
WASSON J. T., WILLIS J., WAI C. M., and KRACHER A. (1980) Origin of iron meteorite groups IAB and IIICD. *Z. Naturforsch.* **35a**, 781–795.
WASSON J. T., OUYANG X., WANG J., and JERDE E. (1989) Chemical classification of iron meteorites—XI. Multielement studies of 38 new irons and the high abundance of ungrouped irons from Antarctica. *Geochim. Cosmochim. Acta* **53**, 735–744.
WIDOM E., RUBIN A. E., and WASSON J. T. (1986) Composition and formation of metal nodules and veins in ordinary chondrites. *Geochim. Cosmochim. Acta* **50**, 1989–1995.
WILKINSON L. (1987) SYSTAT: The System for Statistics. SYSTAT, Inc., Evanston.
WILLIS J. (1980) The mean compositions of iron meteorite parent bodies. Ph.D. thesis, Univ. California, Los Angeles.
WOOD J. A. (1979) Review of the metallographic cooling rates of meteorites and a new model for the planetesimals in which they formed. In *Asteroids* (ed. T. GEHRELS), pp. 849–891. Univ. Arizona Press.

APPENDIX: PETROGRAPHIC DESCRIPTIONS OF MESOSIDERITE METAL NODULES

In these descriptions all modes are in units of vol%. Schreibersite is present in accessory amounts in or next to kamacite except as indicated. Kamacite bandwidths are corrected for geometry.

Bondoc: 25 × 35 mm

The nodule (Fig. 1a) mainly (85%) consists of polycrystalline kamacite; the typical grain size is ~3 mm. Cloudy taenite occurs only as rare ellipsoidal patches (125 × 325 μm) surrounded by 10-μm-thick rims of tetrataenite. Round clumps of silicates (~10%) consist of low-Ca pyroxene, anorthite, and silica with accessory chromite and merrillite. Limonite (~5%) occurs at the edge of the nodule and as thin veins.

Chinguetti: >7 × 12 mm

This troilite-rich nodule (Fig. 1e) consists mainly of 1–4 mm kamacite crystals (75%); no Widmanstätten pattern is present. Cloudy taenite (7%) occurs as 90–180 μm elongated amoeboid patches rimmed by 10 μm tetrataenite (1%). Troilite (15%) forms 0.1–2 mm (typically 0.3–0.6 mm) ellipsoidal inclusions in kamacite or between kamacite and taenite. Some troilite grains contain 50–600 μm polymineralic silicate inclusions (1%).

Crab Orchard: 10 × 15 mm

Polycrystalline kamacite (94%) forms 1–4 mm grains. Cloudy taenite (4%) occurs as 20- to 60-μm subparallel lamellae with 10- to 15-μm tetrataenite rims. Limonite (2%) fills fractures. A few ≤ 100 μm isolated patches of silicates (<1%) consist of low-Ca pyroxene, silica, and anorthite. Accessory troilite, pentlandite, and schreibersite are also present.

Dalgaranga: 10 × 15 mm

The large nodule forms a continuous Widmanstätten pattern, kamacite (73%) occurs as distorted lamellae with the mean width of 0.3 ± 0.1 mm (Fig. 1b). Cloudy taenite (14%) forms ≥ 20 μm patches with 5- to 10-μm tetrataenite (10%) rims. A few 5- to 20-μm tetrataenite lamellae are present. A large, 0.6 × 1.2 mm clump of silicates (1%) consists of low-Ca pyroxene, anorthite, and accessory troilite and Al-rich chromite. Schreibersite (1%) is also present. Limonite (1%) occurs as irregular patches at the edge of the nodule and as thin veins at schreibersite-kamacite and kamacite-kamacite boundaries.

Emery: 3 × 3.5 mm

This is the smallest nodule, and the one with the highest content of silicates. The irradiated sample consists of the metal nodule (75%) and surrounding silicate-rich matrix (25%). The nodule consists of 90% metal, 8% silicates, and 2% limonite. Polycrystalline, 1- to 2-mm, equiaxed kamacite constitutes 85% of the nodule. Cloudy taenite (4%) forms irregular, isolated, 50- to 150-μm patches having 10-μm tetrataenite (1%) rims. Silicates occur as irregular-to-rounded, 100- to 400-μm clumps; tiny (<10 μm) troilite inclusions are associated with the silicates. Limonite occurs as equidimensional ~20-μm grains attached to silicates and as 10- to 20-μm veins filling fractures in the kamacite.

Estherville: 5 × 10 mm

This nodule contains 1% silicate; other inclusions are rare. The metal forms a continuous Widmanstätten pattern; it consisted of a single taenite crystal at high temperatures. Mean kamacite bandwidth is ~0.6 mm. Cloudy taenite forms 20- to 80-μm-thick bands and rare (≤300-μm) amoeboid patches inside and adjacent to kamacite; these are surrounded by 5- to 10-μm tetrataenite rims. Rare 300-μm silicate inclusions near the nodule margin include low-Ca pyroxene, anorthite, silica, and trace amounts of Al-rich chromite.

Mincy: 3.5 × 5 mm

The nodule consists mainly of coarse (>2-mm) equiaxed kamacite (85%); no Widmanstätten pattern is present. Cloudy taenite (4%) occurs as irregular, elongated 0.2- to 2-mm lumps with 10-μm tetrataenite (1%) rims. Silicate clumps (5%) contain low-Ca pyroxene, silica, anorthite, and trace amounts of troilite and chromite. Schreibersite (1%) occurs as elongated 0.1- to 0.5-mm laths at kamacite-kamacite grain boundaries. Limonite (4%) forms irregular patches and fills fractures.

Morristown: 20 × 20 mm

The nodule consists primarily of coarse (2- to 4-mm) equiaxed kamacite (75%) and abundant evenly dispersed 0.3- to 0.5-mm silicate clumps (15%). Cloudy taenite (7%) occurs as 100-μm amoeboid lumps inside large kamacite crystals and at kamacite-kamacite and kamacite-silicate phase boundaries; 10- to 40-μm tetrataenite (3%) surrounds the taenite. The silicate clumps consist of low-Ca pyroxene, anorthite, and trace rutile.

Patwar: 5 × 12 mm

This nodule (Fig. 1d) consists of a 1- to 5-mm-thick peripheral layer of polycrystalline kamacite and a central core exhibiting a Widmanstätten pattern; the mean bandwidth is 150 μm. Kamacite constitutes ~80% of the nodule. Cloudy taenite (3%) typically forms 40-μm bands with 10- to 20-μm tetrataenite (2%) rims. Troilite (10%) occurs as large (up to 1.5 mm) inclusions within kamacite; one large clump is adjacent to a 15- to 60-μm-thick band of tetrataenite. The largest troilite contains silicate grains 10 to 350 μm in size. Silicate clumps (5%) consist principally of low-Ca pyroxene and anorthite; they occur exclusively near the outer edge of the swathing kamacite. It appears that the nodule originally consisted of a single crystal of taenite, and that the swathing kamacite exsolved first, but was later recrystallized.

Pinnaroo: 20 × 20 mm

The nodule (Fig. 1c) consists of 98% metal and 2% schreibersite. Kamacite (88%) has a mean bandwidth of 0.7 ± 0.1 mm and occurs intergrown with cloudy taenite (8%) to form a continuous Widmanstätten pattern. The nodule is surrounded by thick swathing kamacite (Fig. 1c). Cloudy taenite is present in the centers of 30- to 60-μm "taenite" patches (2%).

RKPA79015: >20 mm

RKPA79015 is an unusual mesosiderite consisting of extremely heterogeneous mixtures of silicate and metal (Fig. 6.17 of McSween, 1987). The analyzed sample is mainly comprised of 2- to 4-mm kamacite crystals (75%). Cloudy taenite (17%) surrounded by 10-μm tetrataenite rims forms irregular 30- to 150-μm amoeboid patches. Troilite occurs as minor (6%) rounded 300-μm crystals embedded in kamacite; schreibersite (1%) consists of isolated 60 × 200-μm grains between kamacite crystals and as curved 60-μm-thick bands between kamacite and tetrataenite. There are no silicates in the analyzed sample. This specimen did not form a single taenite crystal at high temperatures.

Vaca Muerta: 12 × 16 mm

This large, 45-g nodule (Fig. 1f) consists mainly (70%) of kamacite lamellae (mean width 0.25 ± 0.05 mm). The Widmanstätten pattern is the most regular among our set of nodules. Cloudy taenite (12%) typically occurs between kamacite lamellae. Some cloudy taenite lamellae are curved, irregular, broken, and embayed, perhaps indicative of cold working in the $\alpha + \gamma$ field followed by reannealing. Tetrataenite (10%) occurs as 5- to 10-μm rims on taenite and as 5- to 20-μm lamellae. Troilite (2%) occurs as minor 0.02- to 3-mm subhedral (hexagonal) to rounded polycrystalline grains; most contain silicate inclusions. Silicates (1%) form 0.2- to 2-mm polymineralic clumps that contain small (<20 μm) troilite inclusions.

Veramin: 4 × 10 mm

This nodule consists mainly of 1- to 4-mm kamacite (88%) and numerous irregular-to-rounded 0.02- to 1-mm clumps of silicate (7%). Cloudy taenite (4%) occurs as rounded and embayed patches (typically 100 μm thick) at kamacite-silicate phase boundaries, and as elongated lamellae (up to 80 × 1200 μm); tetrataenite (1%) forms 5- to 40-μm rims on the cloudy taenite. The silicate clumps consist of major low-Ca pyroxene (bronzite), minor diopside, and anorthite, and accessory 20- to 40-μm patches of merrillite and troilite.